

# A *Spitzer* Census of Star Formation Activity in the Pipe Nebula

Jan Forbrich, Charles J. Lada, August A. Muench

*Harvard-Smithsonian Center for Astrophysics, 60 Garden Street, Cambridge, MA 02138*

jforbrich, clada, amuench@cfa.harvard.edu

and

João Alves

*Calar Alto Observatory, Centro Astronómico Hispano Alemán, C/Jesús Durbán Remón, 2-2, 04004*

*Almeria, Spain*

jalves@caha.es

and

Marco Lombardi

*European Southern Observatory, Karl-Schwarzschild-Str. 2, 85748 Garching, Germany*

m.lombard@eso.org

## ABSTRACT

The Pipe Nebula, a large nearby molecular cloud lacks obvious signposts of star formation in all but one of more than 130 dust extinction cores that have been identified within it. In order to quantitatively determine the current level of star formation activity in the Pipe Nebula, we analyzed 13 square degrees of sensitive mid-infrared maps of the entire cloud, obtained with the Multiband Imaging Photometer for *Spitzer* (MIPS) at wavelengths of 24  $\mu\text{m}$  and 70  $\mu\text{m}$  to search for candidate Young Stellar Objects (YSOs) in the high-extinction regions. We argue that our search is complete for class I and typical class II YSOs with luminosities of  $L_{\text{bol}} \sim 0.2 L_{\odot}$  and greater. We find only 18 candidate YSOs in the high-extinction regions of the entire Pipe cloud. Twelve of these sources are previously known members of a small cluster associated with Barnard 59, the largest and most massive dense core in the cloud. With only six candidate class I and class II YSOs detected towards extinction cores outside of this cluster, our findings emphatically confirm the notion of an extremely low level of star formation activity in the Pipe Nebula. The resulting star formation efficiency for the entire cloud mass is only  $\sim 0.06\%$ .

*Subject headings:* stars: formation — stars: pre-main sequence — infrared: stars

## 1. Introduction

The most critical but least understood aspects of the star formation process concern its initial conditions and earliest stages. In particular, little is known about the initial phases of protostellar development within dense molecular cloud cores and even less is known about the origin of the dense cores themselves. This is largely due to an apparent absence of nearby ( $d < 2.5 \text{ kpc}$ ) massive

( $> 10^4 M_{\odot}$ ) molecular clouds in a sufficiently early evolutionary state so that little or no star formation activity is present within them. This is then taken as evidence that the onset of star formation in molecular clouds is extremely rapid and that clouds in the earliest evolutionary states must be exceedingly rare. Clearly the identification and detailed study of such clouds provides invaluable information about the earliest phases of star for-

mation.

With a mass of  $10^4 M_{\odot}$  and a distance of 130 pc (Lombardi et al. 2006), the Pipe Nebula is one of the massive clouds nearest to the Sun and yet has received little attention and has only been studied in detail within the last few years. With the exception of Barnard 59, the region is lacking the most obvious signposts of star formation, such as bright H II regions, reflection nebulae, luminous infrared sources and large populations of emission-line stars and may be a prime example of a molecular cloud in an early stage of evolutionary development. As such, it constitutes a critical laboratory for star formation studies (for a review, see Alves et al. 2008b). The first wide-area study of the region consisted of CO mapping carried out by Onishi et al. (1999) who identified 14  $C^{18}O$  cores in a large low-resolution and undersampled map. Subsequently, Lombardi et al. (2006) presented a high-resolution completely sampled dust extinction map (based on 2MASS near-infrared data) to study general properties of the cloud. This extinction map was also used to study its dense core population: Alves et al. (2007) identified a population of roughly 150 extinction cores and found that the shape of the core mass function (CMF) is nearly identical to the stellar initial mass function (IMF), but shifted to higher masses by a factor of three, suggesting that the CMF is a direct evolutionary precursor to the stellar IMF. Most recently, Rathborne et al. (2009) have further refined the core identification by taking into account additional measurements of  $C^{18}O$  strength and velocity towards single cores as indicators of dense material and cloud membership. Their list contains 134 dense cores in the Pipe Nebula. To more reliably detect the extinction peaks, Rathborne et al. (2009) have used a background-subtracted version of the near-infrared extinction map, produced by filtering out structures surpassing a given size (see also Alves et al. 2007). Note that in the following, we will generally refer to this background-subtracted map as the extinction map, except as otherwise noted.

The only previously known region of active star formation in the Pipe Nebula is the dark cloud Barnard 59 (B 59, Barnard 1927). Early studies found indications of ongoing star formation in B 59: H $\alpha$  emission line stars (Herbig 2005, and references therein), a millimeter continuum

source (Reipurth et al. 1996), and a CO outflow (Onishi et al. 1999). More recently, *Spitzer* observations revealed a young cluster inside of B 59 (Brooke et al. 2007). Riaz et al. (2009) studied the cluster's most deeply embedded object, [BHB2007] 11, in more detail. In order to quantify the star formation activity for the whole cloud complex, we present a mid-infrared survey carried out with the Multiband Imaging Photometer for *Spitzer* (MIPS) as well as with the Infrared Array Camera (IRAC), both onboard the *Spitzer* Space Telescope.

## 2. Observations and Data Reduction

We present large-area mapping observations of the Pipe Nebula, carried out with *Spitzer*-MIPS (Rieke et al. 2004), at wavelengths of 24  $\mu\text{m}$  and 70  $\mu\text{m}$ . The observations were obtained between April 2004 and October 2006. The data consist of 44 Astronomical Observation Requests (AORs). They come from three different programs: the Cycle 1 GTO observations of B68 (Program Identification PID 53, 1 AOR), six mipsphot observations from Legacy observations (PID 139, c2d) and 35 mipsscan as well as 3 mipsphot maps from the Cycle 2 GO Pipe Cloud Survey (PID 20119). We use *Spitzer*-IRAC data that were mostly collected as part of program PID 20119, but also as programs PID 139 and PID 30570. The observations were designed to cover the most highly extinguished regions of the Pipe Nebula. In total, the 24  $\mu\text{m}$  data cover an area of 13.4 square degrees, with the 70  $\mu\text{m}$  data covering a very similar area (to within 2%).

The data reduction was performed with the MOPEX software package, v18.1.5<sup>1</sup>. The 24  $\mu\text{m}$  data were self-calibrated by dividing each Basic Calibrated Data (BCD) image with a flatfield created by stacking all the BCDs in an AOR. All MIPS BCDs were from release S16. Self calibration in this way removes large scale sky variations and some artifacts. The flat field image was created and applied using the flatfield.pl tool provided as part of MOPEX. Briefly, the BCD stack are median filtered in order to detect sources, mask bright sources, and then median stack the original frames into a flat, clipping out the bright sources. No overlap correction was applied to the

<sup>1</sup><http://ssc.spitzer.caltech.edu/postbcd/mopex.html>

24  $\mu\text{m}$  data since flatfielding appeared to be sufficient. The AORs were individually processed into mosaics to preserve the two-epoch nature of most of the 24  $\mu\text{m}$  data, allowing the rejection of asteroids in the final source catalog. The mosaicking produced images with a final pixel size of  $2.5''$  and included steps to mask faulty bits and reject outliers. No self-calibration or overlap corrections were applied to the 70  $\mu\text{m}$  BCDs where we work with the median-filtered (fbcd) frames produced by the Spitzer Science Center pipeline process. The pixel size at 70  $\mu\text{m}$  is  $4''$ .

Source detection was performed on the individual 24  $\mu\text{m}$  mosaics, using MOPEX multi-frame PRF-fitting photometry. Given the Pipe Nebula's location close to the ecliptic and thus an increased probability to detect asteroids, we required source detections in both of the two observation epochs, if two observing epochs were available. The concatenated list of source detections contains nearly 80000 sources above a signal-to-noise ratio of four. In contrast, the 70  $\mu\text{m}$  map mostly has only single-epoch coverage. Source detection was carried out on a single, large map produced from the median-filtered BCD files. In this map, a total of 5308 sources were detected above a signal-to-noise ratio of four. A cross-correlation of the two lists with a search radius of  $4''$  yields a list of 546 sources detected in both MIPS bands.

For the identified candidate YSOs, we obtained *Spitzer*-IRAC mid-infrared aperture photometry from corresponding post-basic calibrated data (PBCD) sets for use in the fitting of their spectral energy distributions (SEDs), allowing a photometric accuracy of  $\sim 10\%$ . Post-BCD mosaics from the Spitzer Science Center (pipeline S14) were used without modification. Aperture radii used were either two or three pixels (the former only for sources 22 and 24 to exclude neighboring sources), with a pixel size of  $1.2''$  and the corresponding aperture corrections. In a few cases, this required the use of a tool<sup>2</sup> to rectify saturated sources.

While we processed and analyzed the crowded young cluster region Barnard 59 in the same way as all other data, we make use of the IRAC and MIPS photometry from Brooke et al. (2007) for two reasons: first, the crowding is especially prob-

lematic in the MIPS data that we use for source detection, causing us to miss a few sources. However, no comparable crowding occurs in the entire remaining areas in the Pipe Nebula. Second, the most clearly saturated sources are in B 59, requiring more effort to extract reliable photometry. As was pointed out by Brooke et al. (2007), the three brightest 24  $\mu\text{m}$  sources in B 59 ([BHB2007] 1, 7, and 11) are saturated while at 70  $\mu\text{m}$ , only [BHB2007] 11 is saturated. Outside of B 59, among the sources we are studying, only KK Oph is saturated at 24  $\mu\text{m}$ .

In addition to crowding of bright sources, our reliance on MIPS data for the identification of YSOs also suffers from the relatively low angular resolution: the detectability of multiple systems is reduced even when compared to 2MASS. For example, KK Oph is a known binary with a separation of  $1.6''$  (see below), but we cannot resolve the two components.

### 3. Analysis

#### 3.1. Selection of candidate YSOs

We expect to find any candidate protostars in the relatively high-extinction regions of the cloud. These regions correspond to only a small percentage of the full coverage. In line with earlier analysis (Rathborne et al. 2009, in particular), we use the following threshold to define the high-extinction regions: in an extinction map in which extended structure has been removed by means of wavelet subtraction (Alves et al. 2007) we use a minimum extinction of  $A_V > 1.2$  mag. An area of 0.98 square degrees is above this threshold out of which the identified dense cores (Rathborne et al. 2009) comprise an area of 0.75 square degrees. In the following, we will constrain the star formation activity in these high-extinction regions. It will become clear that we can constrain the sizes of the populations of both class I protostars and class II YSOs (as defined by Lada 1987) in the high-extinction regions.

Given the location of the Pipe Nebula, projected onto the vicinity of the Galactic center, the background source density in the region is enormous and selection criteria for candidate YSOs are of particular importance. Compared to source detection at near-infrared wavelengths, the lower source density in the mid-infrared at 24  $\mu\text{m}$  and

<sup>2</sup><http://spider.ipac.caltech.edu/staff/jarrett/irac/tools/>

70  $\mu\text{m}$  allows us to work with a sensitivity-limited (rather than confusion-limited) sample of objects. When looking for candidate protostars at these wavelengths, we first have to establish whether the mid-infrared mosaics are sensitive enough for this purpose. A good first test is to look at the lowest-luminosity protostellar objects known, the Very Low Luminosity Objects (VeLLOs). These objects were only discovered recently, with the unprecedented sensitivity of *Spitzer*. The four VeLLOs that have been studied in detail (Young et al. 2004; Bourke et al. 2006; Dunham et al. 2006; Lee et al. 2009, , L1014-IRS, L1521F-IRS, IRAM 04191, and L328-IRS, respectively) have been detected with MIPS at both 24  $\mu\text{m}$  and 70  $\mu\text{m}$ , and their mean bolometric luminosity is 0.25  $L_{\odot}$  (the extreme values being 0.15  $L_{\odot}$ , IRAM 04191, and 0.36  $L_{\odot}$ , L1521F-IRS). Note that the bolometric luminosities are significantly higher than the intrinsic luminosities of the corresponding central objects. Detections at both 24  $\mu\text{m}$  and 70  $\mu\text{m}$  are also used as criteria by Dunham et al. (2008) who list a total of 15 candidate VeLLOs as a result of surveying the *Spitzer* c2d data. The fact that the four above-mentioned VeLLOs are located nearby and at least as distant as the Pipe Nebula means that we can use them to define flux cut-off values at both 24  $\mu\text{m}$  and 70  $\mu\text{m}$  to include these currently known VeLLOs. These flux limits ensure that we can detect even the lowest-mass protostellar objects.

As our first selection criterion we thus require candidate YSOs to have flux densities of at least 10 mJy at 24  $\mu\text{m}$  and 100 mJy at 70  $\mu\text{m}$ . It turns out that both cut-off values are comfortably above the detection limits in both bands. In the list of sources detected in both MIPS bands, the typical photometric uncertainties determined by MOPEX are 0.09 mJy at the 24  $\mu\text{m}$  flux cutoff and 5.65 mJy at the 70  $\mu\text{m}$  flux cutoff. As a second step, we are using a direct application of the original definition of YSO SED classes of Lada (1987), although implemented in longer-wavelength (MIPS) bands. Thus, we require a positive spectral index,  $\alpha = d\log\lambda F_{\lambda}/d\log\lambda$ , in the two MIPS bands, in order to find the earliest (class I) protostellar stages. In this case, a positive spectral index in  $\lambda F_{\lambda}$  corresponds to a flux ratio of  $F_{\nu}(70\mu\text{m})/F_{\nu}(24\mu\text{m}) > 70/24$ . A similar criterion can be used to select candidate class II sources, dominated by their disk

emission. They are expected to have flux ratios of  $F_{\nu}(70\mu\text{m})/F_{\nu}(24\mu\text{m}) > 1/3$ , corresponding to a spectral index of  $\alpha > -2$ . Sources above our flux cut-off values but below this minimum spectral index include candidate class III sources. Since these presumably become difficult to distinguish from stellar photospheres of field stars, we do not discuss these in further detail, focusing only on candidate class I and II sources as possible products of recent star formation. Only these sources, as defined by our MIPS-based criteria, will be referred to in the following as candidate YSOs.

Using these criteria, we identify in Fig. 1 a total of only 25 candidate YSOs in the high-extinction regions of the entire complex, 12 of which are located in B 59. These sources were matched with the 2MASS point source catalog, using a search radius of 3". The median difference in position is 1.5". We found one additional candidate YSO in a region without coverage at 70  $\mu\text{m}$ . This source is listed as candidate 26. Lacking 70  $\mu\text{m}$  coverage, source 26 was identified by its  $K_S - [24]$  color of  $10.459 \pm 0.082$  mag. There are no further sources with comparably extreme  $K_S - [24]$  colors that are not already covered by the above criteria. Given the superior sensitivity of the above method, which does not depend on near-infrared detections, we do not further discuss  $K_S - [24]$  colors. The resulting 26 candidate YSOs and their photometry are listed in Tables 1 and 2, sorted by descending 70 $\mu\text{m}$  flux. The photometric errors consist of the fitting errors reported by MOPEX, with the absolute errors<sup>3</sup> added in quadrature (for the saturated sources, a larger error is assumed). In order to allow us to compare the photometry, we have added these absolute uncertainties also to the errors reported by Brooke et al. (2007) for the non-saturated sources, since the errors in their source table are the formal fitting errors. For all candidate YSOs we confirmed their detection in two different epochs of MIPS24 observations, ensuring that they were not caused by asteroids. Source 26 was confirmed by the presence of a mid-infrared IRAC counterpart.

For B 59, when applying our criteria to the 12 sources from Brooke et al. (2007) that have MIPS24 and MIPS70 photometry, we find four

<sup>3</sup>4% at 24  $\mu\text{m}$  and 7% at 70  $\mu\text{m}$ , according to MIPS Data Handbook V3.3.1

candidate class I sources and eight candidate class II sources. This leaves eight sources from the Brooke et al. (2007) list of 20 that do not appear to qualify as candidate YSOs according to our MIPS-based criteria. While in some cases, these objects are genuinely excluded by our method, in other cases, no suitable MIPS photometry is available. One of these sources, [BHB2007] 20 is not covered at  $70 \mu\text{m}$  so that it is not selected by our criteria. Three sources ([BHB2007] 2, 6, and 12) are too close to bright neighboring sources for any reliable photometry in either of the MIPS bands to be extracted (and no such photometry is listed in Brooke et al. 2007); therefore, these sources do not appear in our list. The remaining four sources are the outermost objects which are not detected at  $70 \mu\text{m}$ ; only upper limits were given by Brooke et al. (2007). These include [BHB2007] 5 and 17, which Covey et al. (2009) determined to be background giants, using near-infrared spectroscopy. The source [BHB2007] 17 is very close to the chip edge in the  $70 \mu\text{m}$  coverage, and not detected in spite of its bright  $24 \mu\text{m}$  counterpart.

The sensitivity of our MIPS mosaics, as we have argued, is enough to even detect VeLLOs at the distance of the Pipe Nebula. Therefore, we estimate that our survey is complete for candidate class I protostars of  $L > 0.2 L_{\odot}$ . We note that even for candidate class II sources, our selection method is very sensitive. Note that we used a conservative limit of  $\alpha_{24-70} > -2$  to *find* all possible candidate class II sources. This index corresponds to the ideal case of an optically thick, spatially flat disk. In reality, observed class II SEDs often have significantly flatter slopes due to disk flaring and viscous heating, resulting in  $\alpha = -0.7 \pm 0.3$  (Kenyon & Hartmann 1987, for a spectral range of  $2 - 60 \mu\text{m}$ ). In Section 3.4, when we study their SEDs, we will see from the final classification (Table 4) that our candidate class II sources have a median<sup>4</sup> spectral index of  $\alpha_{K-24} = -0.73$ . We can thus roughly estimate the completeness for such typical class II sources by comparing with an observed example, the fluxes of FM Tau, a K3 class II source ( $\alpha_{K-24} = -0.65$ ) in Taurus at a similar distance as the Pipe. FM Tau has a total luminosity of  $0.5 L_{\odot}$  (e.g., Strom et al. 1988)

<sup>4</sup>The values range from  $\alpha_{K-24} = -0.54$  to  $\alpha_{K-24} = -0.83$ , leaving aside source 24 with a markedly double-peaked SED ( $\alpha_{K-24} = -1.47$ ).

and a  $70 \mu\text{m}$  flux density of  $0.29 \text{ Jy}$  (from the Taurus Spitzer Legacy Project). Scaling that to our flux density cut-off at  $70 \mu\text{m}$  ( $0.1 \text{ Jy}$ ) and assuming the same distance for the sake of this comparison yields a completeness limit for class II SEDs of only  $L_{\text{bol}} \sim 0.2 L_{\odot}$ . The flux density ratio  $F_{\nu}(70 \mu\text{m})/F_{\nu}(24 \mu\text{m})$  in this case is 0.59. A similar check with two late-type class II objects, FN Tau (M5,  $\alpha_{K-24} = -0.53$ ) and FP Tau (M2.5,  $\alpha_{K-24} = -1.12$ ), yields even lower limiting luminosities for our flux limits (i.e.,  $0.05 L_{\odot}$  and  $0.12 L_{\odot}$ , respectively), corroborating our estimate of  $L_{\text{bol}} \sim 0.2 L_{\odot}$ . The completeness level for typical observed class II sources is comparable to the one for class I protostars discussed above.

While all candidate sources by definition are in regions with  $A_V > 1.2 \text{ mag}$  (in the extinction map without extended structure, see above), not all of them are projected onto what Rathborne et al. (2009) define as dense cores, see Table 1. Five of our sources either lie in extinction cores that do not fulfill the minimum size requirement set by Rathborne et al. (2009) or were excluded due to their  $\text{C}^{18}\text{O}$  emission properties: One source is close to an extinction peak without detected  $\text{C}^{18}\text{O}$  emission (source 16), and, most interestingly, the extinction core onto which source 17 is projected, as well as its neighboring cores, have  $\text{C}^{18}\text{O}$  emission at a velocity that is significantly different from the cloud velocity ( $v = 21 \text{ km s}^{-1}$  vs. a range for the Pipe Nebula of  $v = 2.8 \text{ km s}^{-1}$ , Rathborne et al. 2009). This candidate YSO therefore apparently does not belong to the Pipe Nebula complex. For the five cases where cores and their masses are not listed by Rathborne et al. (2009), Table 1 lists corresponding mass estimates, derived according to the procedure outlined in Section 3.6. These estimates take into account all pixels of the background-subtracted extinction map with  $A_V > 1.2 \text{ mag}$  if they have not been assigned to neighboring cores. Note that some of the changes in the refined core list are due to the intricacies of defining the core population, a process that is not unambiguous.

### 3.2. Comparison to control regions

While we have estimated the sensitivity of our selection method, we still have to determine the amount of contamination by background sources. As control region, we use those parts of our MIPS

mosaics that are not covering the high-extinction regions, i.e., regions with  $A_V < 1.2$ . Applying the selection criteria to these sources allows us to approximately predict how many detections in each category could be due to background objects and to judge whether the number of identified candidates exceeds the number of expected background sources. As mentioned above, about 94% of our map is not covering high-extinction regions. Given the proximity of the Pipe Nebula to the Galactic center, there is a high density of background sources, presumably mainly in the Galactic bulge. While 56 sources were detected at both  $24\ \mu\text{m}$  and  $70\ \mu\text{m}$  in regions with extinctions above 1.2 mag (not applying any filtering), 490 such sources were detected in the remainder of the map. Fig. 2 depicts the sources in the control region in the same way as the high-extinction sources were plotted in Fig. 1. Some of the sources in the control region technically fulfill our candidate YSO selection criteria, indicating that there is contamination in our list of candidate YSOs. Table 3 contains a comparison of the control region and the high-extinction regions in the Pipe Nebula in terms of candidate YSOs. Taking into account that regions with extinctions above 1.2 mag cover only  $\sim 7\%$  of the map (see above), we find that that in the three ranges of flux ratios corresponding to YSOs, we find more candidates than can be expected from background contamination alone. In particular, and most importantly, we detect nine candidate class I sources while the expected background contamination is 2.9 sources. This relative overdensity of candidate YSOs in the high-extinction regions suggests that their occurrence is indeed related to the presence of dense material and supports the notion that some of these objects really are YSOs.

### 3.3. Comparison to other star-forming regions

There are two obvious possibilities to compare the application of our candidate YSO identification method to other star-forming regions. First of all, given its location at about the same distance, it is interesting to compare the Pipe Nebula to the Taurus star-forming region. While a full application of our method to the Taurus data is beyond the scope of this paper, we can at least check whether known objects occupy the region of flux

space that we use to identify candidate YSOs. In a preliminary version of their source list, the Taurus Spitzer legacy project<sup>5</sup> lists 693 sources that are detected at both  $24\ \mu\text{m}$  and  $70\ \mu\text{m}$ , a precondition for our candidate YSO selection method. The Taurus map covers a total of about 40 square degrees, four times larger than our map of the Pipe Nebula. We correlate the *Spitzer* source list with the list of YSOs in Taurus-Auriga given by Kenyon et al. (2008). This table contains 383 low-mass YSOs of which 98 have counterparts in the *Spitzer* list with detections in both MIPS bands (within a search radius of  $1''$ , see above; note that the two lists cover different areas). The Kenyon et al. list does not distinguish the different evolutionary stages, but as shown in Fig. 3, this selection of sources is well constrained by the regions in the  $70\ \mu\text{m}$  vs.  $24\ \mu\text{m}$  plot that we use for the selection of candidate YSOs. To illustrate that prototypical class I sources fall into the corresponding selection region, we note that L1551 IRS5 (not covered by the Taurus Spitzer Legacy Project), already based on its IRAS data, fulfills the criteria, but lies outside of our plot limits due to its brightness: its  $60\ \mu\text{m}$  flux is 373 Jy, and its  $25\ \mu\text{m}$  flux is 106 Jy, i.e., the flux ratio is 3.5. This example once more underlines the sensitivity of the *Spitzer* MIPS observations.

For a second comparison, we consider the candidate YSOs that have been identified by the “Cores to disks” (c2d) Spitzer Legacy Project. This comparison is different, since it allows us to select already identified candidate YSOs and look at their properties at  $24\ \mu\text{m}$  and  $70\ \mu\text{m}$ . The c2d “Ensemble Cores” list of candidate YSOs contains 106 objects with both  $24\ \mu\text{m}$  and  $70\ \mu\text{m}$  fluxes out of 122 candidate YSOs that were observed at both wavelengths<sup>6</sup>. Reassuringly, when we plot the sources in the same way as we plotted the candidate YSOs in the Pipe, the sources roughly fall into the region of flux space where we expect candidate YSOs in the Pipe cloud (Fig. 3). This is reassuring since the MIPS spectral index is not part of the selection criteria that were used by the c2d team. Note that the data have not been corrected for the different

<sup>5</sup>[http://data.spitzer.caltech.edu/popular/taurus2/20081007\\_enhanced/](http://data.spitzer.caltech.edu/popular/taurus2/20081007_enhanced/)

<sup>6</sup>Sixteen sources are listed as “undetected” at  $70\ \mu\text{m}$ , but are located in the vicinity of other, mostly bright,  $70\ \mu\text{m}$  sources, complicating their detection.

distances ( $\sim 120\text{--}250$  pc) of the several different nearby star-forming regions that were part of the survey.

These two examples demonstrate that using the  $24\ \mu\text{m}$  and  $70\ \mu\text{m}$  MIPS bands and their high sensitivity constitutes a powerful method to look for candidate YSOs in the Pipe cloud. The drawback of relatively low angular resolution is in our case overcompensated by the enormous reduction of sources to survey (while keeping a high sensitivity) compared to the use of IRAC data which in this direction of the Galaxy are affected by source crowding.

### 3.4. A closer look at the candidate YSOs

A cross-correlation of the 26 candidate YSOs with catalogs, using SIMBAD and VizieR, allows us to identify a first subset of sources that can be rejected as YSO candidates. Source 10 is a 1.4 GHz radio continuum source in the NRAO VLA Sky Survey and listed as a possible pre-planetary nebula by Kohoutek (2001). Sources 13, 14, and 15 are all listed as high mass-loss asymptotic giant branch stars by Ojha et al. (2007). After a comparison with typical *Spitzer* galaxy SEDs, in particular looking at the influence of PAH features on the IRAC photometry (e.g., Rowan-Robinson et al. 2005), three additional sources, namely 19, 20, and 22 have been rejected as being likely galaxies. We note that their IRAC colors are  $[5.8\ \mu\text{m}]-[8.0\ \mu\text{m}]>2$  and  $[3.6\ \mu\text{m}]-[4.5\ \mu\text{m}]<0.9$ , supporting this conclusion (e.g., Robitaille et al. 2008). Source 25 looks photospheric except for its  $70\ \mu\text{m}$  flux which is the weakest in this selection. In fact, the  $70\ \mu\text{m}$  detection is surrounded by weak extended emission leading to an overestimate of the flux in the PRF fit. The source has been rejected as not being a true excess source; it is clearly not a class I or class II YSO. The use of catalogs also allows us to confirm the selection of a YSO: source 5 is the Herbig AeBe star KK Oph which is very likely associated to B 59; it appears to have a T Tau companion (Herbig 2005; Carmona et al. 2007). Additionally, Covey et al. (2009) have analyzed near-infrared spectroscopy of our sources 11 and 16, confirming only the latter as a YSO (their source 2, a binary system unresolved in our data), while leaving open the identification of the former (source 1 in their designation). Riaz et al. (2009)

confirm the protostellar nature of source 1. Thus, after this first cross-correlation with catalogs and previously obtained data as well as comparison to galaxy SEDs, 18 candidate YSOs remain, only six of them outside of B 59. We note that the two Brooke et al. (2007) sources rejected as giant stars by Covey et al. (2009), [BHB2007] 5 and 17, are not detected at  $70\ \mu\text{m}$  and thus did not appear in our list.

In order to better characterize the candidate YSOs, we have determined their infrared SEDs, based on 2MASS, IRAC and MIPS photometry. For comparison, we have also determined SEDs for some sources in the control regions that would qualify as candidate YSOs. Subsequently, to test whether the SEDs can be explained as protostellar, we have attempted to fit the SEDs of candidate YSOs with models from Robitaille et al. (2007). These pre-computed radiative-transfer models cover a large region of parameter space. Since most of the sources are relatively bright 2MASS sources and thus do not look like edge-on disk configurations, we excluded such models in the grid from the fitting process, realizing that all SEDs can still be well fitted and explained. For the fits, photometric errors larger than the nominal errors were assumed: 0.1 mag for 2MASS and 10% for all *Spitzer* photometry except for data corrected for saturation, where we assume 20%. The SEDs and fit results are shown in Figs. 4, 5, and 6. Table 4 lists the range of total extinction and the range of bolometric luminosities for all candidate YSOs. The parameter ranges are simply giving the extreme values for all fits within a relatively strict goodness-of-fit criterion<sup>7</sup>,  $\chi^2 - \chi_{\text{best}}^2 < n_{\text{data}}$ . The fit results show that the candidate YSOs can be reasonably described as a mostly low-mass YSO population. The lowest-luminosity candidate class I protostar, source 26, might be a VeLLO in its own right. Also, the lowest luminosities deduced from the model fits are of the same order as our estimated completeness limit.

We use the full SEDs and the model fits to reexamine and refine our initial classification of the candidate YSOs which was based solely on

<sup>7</sup>For source 9, only a single fit was found with this criterion; we therefore relax the criterion for only this source to  $\chi^2 - \chi_{\text{best}}^2 < 2n_{\text{data}}$ .

the MIPS spectral index. In particular, Figs. 4 and 5 show that two candidate YSOs, sources 9 and 24, initially identified as candidate class I sources, exhibit complex double-peaked SEDs that cannot be adequately described by a single spectral index. The full SEDs show, however, that these two sources are more aptly described as class II objects. Additionally, an examination of the SEDs of sources initially selected as candidate class II objects shows that several of these have SEDs that are flatter than expected for prototypical class II objects with shapes similar to those of the flat-spectrum protostellar class defined by Greene et al. (1994). Since their SEDs are well-behaved, we use the wide  $K-24\mu\text{m}$  spectral index, as described in a footnote to Table 2, to refine our classification to include flat-spectrum protostars. The refined YSO classifications are listed in Table 2.

In an attempt to characterize the 48 control sources that technically fulfill our criteria for being candidate class I protostars, we used SIMBAD to identify counterparts. Such counterparts are found for only nine sources within a search radius of  $4''$ . Eight of these appear to be planetary nebulae and one is an OH/IR star. These 48 sources have a mean extinction of 0.1 mag in the extinction map where extended structure has been removed, and a mean extinction of 4.0 mag in the full extinction map. A sample of control SEDs is shown in Fig. 6. While many sources remain unidentified and the multi-wavelength coverage is not the same for all of these objects, most of the sampled sources appear to be galaxies based on their SED shapes, following the same arguments also used in rejecting candidate YSOs above (mainly the influence of PAH features on the IRAC photometry).

### 3.5. Location of the candidate YSOs relative to extinction peaks

Very young candidate YSOs would most likely be found at or in close proximity of the extinction peaks. Fig. 7 shows the identified candidate YSOs overlaid onto the corresponding sections of the extinction map. Given that the candidate YSOs were selected for being inside areas of the extinction map that are above a minimum threshold, it is not surprising to see them close to the extinction peaks, but few are centered on peaks, the best case being source 26. Since one

would expect the youngest sources (class I) to be located at or very near to the extinction peaks, the observed offsets indicate that the candidate YSOs are likely predominantly in later evolutionary stages (i.e., class II). This is compatible with our flux-based characterization which found that most of the candidate YSOs are class II rather than class I (see above). It is interesting to note that while five of the six candidate YSOs outside of B 59 are within  $2.3^\circ$  of the cluster, a single candidate (source 17) is  $5.9^\circ$  away, at the “opposite end” of the cloud. We note again that the corresponding core as well as the surrounding cores were rejected by Rathborne et al. (2009) as being part of the Pipe complex since their  $\text{C}^{18}\text{O}$  velocities are significantly offset from the system velocity. While source 17 nevertheless is a candidate YSO, it probably does not belong to the Pipe Nebula complex. Fig. 8 shows the six candidate YSOs outside of B 59 on the extinction map from Lombardi et al. (2006). It is indeed interesting to note that most of them are located in the “stem” of the Pipe, none having been detected in the “bowl”, even though there are regions of considerable extinction in that area. This suggests that the area around B 59 at the tip of the stem is the most evolved region, followed by the stem, leaving the entire “bowl” in a very early evolutionary stage. Interestingly, this is in line with the conclusions of Alves et al. (2008a) who presented an optical polarization study of the Pipe Nebula. From a strong polarization gradient across the Pipe Nebula, with the lowest amounts of polarization found towards B 59, they propose a very similar picture. While they also suggest that the entire “bowl” region is in a very early stage, they conclude that the “stem” is about to form stars while B 59 has actively ongoing star formation.

### 3.6. Star formation efficiency in the Pipe Nebula

In total, we have found 21 candidate YSOs in the Pipe Nebula. Fifteen<sup>8</sup> of these are in B 59 and only six in the entire remaining cloud complex. Star formation efficiencies (SFEs) are usu-

---

<sup>8</sup>In addition to the 12 MIPS-selected candidate YSOs, we consider the three above-mentioned Brooke et al. (2007) sources in B 59 for which no photometry could be obtained due to nearby bright neighbors, yielding an upper limit of 15 YSOs in B 59.



ally given as  $SFE = M_*/(M_* + M_{\text{cloud}})$ , i.e., they are compared to the total mass of the cloud (in this case,  $M \sim 10^4 M_\odot$ , Onishi et al. 1999). Assuming stellar masses of  $\sim 0.3 M_\odot$  each, this translates into an extremely low star formation efficiency when compared to the mass of the entire cloud, it is only  $\sim 0.06\%$ . Typical values are a few percent; the median of 2% given by Myers et al. (1986) is 33 times higher than our value for the Pipe Nebula.

Furthermore, we can estimate the star formation efficiency for the densest material, considering that the high-extinction regions represent the dense component of the cloud. We can estimate the corresponding cloud mass from the summed pixels in the extinction map, taking into account the high-extinction regions with  $A_V > 1.2$  mag (in the background-corrected map) that were surveyed for candidate YSOs:

$$M = \mu m_{\text{H}} \beta A_{\text{pix}} \Sigma A_V \quad (1)$$

Here,  $\mu$  is the mean molecular weight (1.37),  $m_{\text{H}}$  is the mass of the hydrogen atom,  $\beta$  is the conversion from optical extinction to column density, and  $\Sigma A_V$  is the summed optical extinction.  $A_{\text{pix}}$  is the area of a pixel in  $\text{cm}^{-2}$  at the distance of the source, for extinction pixels with a side length of  $s_{\text{pix}}$  [']:  $A_{\text{pix}} = (\pi/180/3600)^2 s_{\text{pix}}^2 d^2$ , where  $d$  is the distance in cm. While there are 14066 pixels in the extinction map above a threshold of  $A_V > 1.2$  mag (each of size  $30'' \times 30''$ ), only 11063 of these are covered by both the 24  $\mu\text{m}$  and the 70  $\mu\text{m}$  maps. The summed  $A_V$  in these pixels is 29751 mag. Using a conversion factor of  $\beta = 2 \times 10^{21} \text{ cm}^{-2} \text{ mag}^{-1}$  (e.g., Bohlin et al. 1978), the resulting mass is  $230 M_\odot$ . Assuming an upper limit of 21 candidate YSOs, each approximately of  $\sim 0.3 M_\odot$ , again yields an extremely low star formation efficiency of 2.7% when compared to the densest material. This is considerably lower than typical values for clusters which are on the order of 10–40% (e.g., Lada & Lada 1991). We note that at most five of the identified 134 extinction cores (or 3.7%) have candidate YSOs, not counting three additional candidate YSOs in extinction cores projected onto high-extinction regions not part of cores as defined by Rathborne et al. (2009). For the combined data of the *Spitzer* c2d project, the average star formation efficiency is 4.8% while

it is much higher when compared to the dense material, as derived from dust continuum observations (Evans et al. 2009).

#### 4. Summary

We have used very sensitive mid-infrared mapping of the Pipe Nebula to obtain a sensitive census of its extremely low star formation activity. Using the 24  $\mu\text{m}$  and 70  $\mu\text{m}$  MIPS bands to identify candidate YSOs is a powerful tool, allowing us to search the cloud for protostars down to objects with very low luminosities. For both class I and typical class II YSOs the search is estimated to be complete down to luminosities of  $\sim 0.2 L_\odot$ . The star formation efficiency in the Pipe Nebula is only  $\sim 0.06\%$  when compared to the total cloud mass and 2.7% when compared to the mass of the high-extinction regions. This is more than an order of magnitude lower than in typical star-forming regions. Candidate YSOs are found in at most five of the 134 identified extinction cores, leaving the overwhelming majority of cores apparently starless. Outside of Barnard 59, where a previously known cluster of YSOs resides, we find only six new candidate YSOs in the entire remaining Pipe Nebula, one of which has already been confirmed as a YSO by near-infrared spectroscopy (Covey et al. 2009, in prep.). One of these candidate YSOs very likely is not a member of the Pipe Nebula complex. Using our MIPS-based selection criteria, we find an upper limit of 15 candidate YSOs in B 59, all of them previously known. Interestingly, the Pipe candidate YSOs outside of B 59 are not evenly distributed over the remaining cloud, but they are within  $2.3^\circ$  of B 59, leaving large regions of the cloud, particularly the bowl region, without any candidate YSOs. These results clearly demonstrate that apart from B 59, the Pipe Nebula is a region with extremely low star formation activity. We conclude that it appears to be an ideal region to study the initial conditions and earliest stages of star formation.

We would like to thank Thomas Robitaille for help with the SED fits. This work is based on observations made with the Spitzer Space Telescope, which is operated by the Jet Propulsion Laboratory, California Institute of Technology under a contract with NASA. Support for this work was

provided by NASA through an award issued by JPL/Caltech, contract 1279166. This publication makes use of data products from the Two Micron All Sky Survey, which is a joint project of the University of Massachusetts and the Infrared Processing and Analysis Center/California Institute of Technology, funded by the National Aeronautics and Space Administration and the National Science Foundation.

*Facilities:* SST (MIPS), SST (IRAC)

## REFERENCES

- Alves, F. O., Franco, G. A. P., & Girart, J. M. 2008a, *A&A*, 486, L13
- Alves, J., Lombardi, M., & Lada, C. J. 2007, *A&A*, 462, L17
- Alves, J. F., Lombardi, M., & Lada, C. J. 2008b, in *Handbook of Star Forming Regions*, Vol. II, ed. B. Reipurth, 415
- Barnard, E. E. 1927, *Catalogue of 349 dark objects in the sky*, Chicago: University of Chicago Press
- Bohlin, R. C., Savage, B. D., & Drake, J. F. 1978, *ApJ*, 224, 132
- Bourke, T. L., Myers, P. C., Evans, II, N. J., et al. 2006, *ApJ*, 649, L37
- Brooke, T. Y., Huard, T. L., Bourke, T. L., et al. 2007, *ApJ*, 655, 364
- Carmona, A., van den Ancker, M. E., & Henning, T. 2007, *A&A*, 464, 687
- Dunham, M. M., Crapsi, A., Evans, II, N. J., et al. 2008, *ApJS*, 179, 249
- Dunham, M. M., Evans, II, N. J., Bourke, T. L., et al. 2006, *ApJ*, 651, 945
- Evans, N. J., Dunham, M. M., Jørgensen, J. K., et al. 2009, *ApJS*, 181, 321
- Greene, T. P., Wilking, B. A., Andre, P., Young, E. T., & Lada, C. J. 1994, *ApJ*, 434, 614
- Herbig, G. H. 2005, *AJ*, 130, 815
- Kenyon, S. J., Gómez, M., & Whitney, B. A. 2008, *Low Mass Star Formation in the Taurus-Auriga Clouds (Handbook of Star Forming Regions, Volume I: The Northern Sky ASP Monograph Publications, Vol. 4. Edited by Bo Reipurth)*, 405
- Kenyon, S. J. & Hartmann, L. 1987, *ApJ*, 323, 714
- Kohoutek, L. 2001, *A&A*, 378, 843
- Lada, C. J. 1987, in *IAU Symposium, Vol. 115, Star Forming Regions*, ed. M. Peimbert & J. Jugaku, 1–17
- Lada, C. J. & Lada, E. A. 1991, in *Astronomical Society of the Pacific Conference Series, Vol. 13, The Formation and Evolution of Star Clusters*, ed. K. Janes, 3–22
- Lee, C. W., Bourke, T. L., Myers, P. C., et al. 2009, *ApJ*, 693, 1290
- Lombardi, M., Alves, J., & Lada, C. J. 2006, *A&A*, 454, 781
- Myers, P. C., Dame, T. M., Thaddeus, P., et al. 1986, *ApJ*, 301, 398
- Ojha, D. K., Tej, A., Schultheis, M., Omont, A., & Schuller, F. 2007, *MNRAS*, 381, 1219
- Onishi, T., Kawamura, A., Abe, R., et al. 1999, *PASJ*, 51, 871
- Rathborne, J. M., Lada, C. J., Muench, A. A., et al. 2009, *ApJ*, 699, 742
- Reipurth, B., Nyman, L.-A., & Chini, R. 1996, *A&A*, 314, 258
- Riaz, B., Martín, E. L., Bouy, H., & Tata, R. 2009, *ApJ*, 700, 1541
- Rieke, G. H., Young, E. T., Engelbracht, C. W., et al. 2004, *ApJS*, 154, 25
- Robitaille, T. P., Meade, M. R., Babler, B. L., et al. 2008, *AJ*, 136, 2413
- Robitaille, T. P., Whitney, B. A., Indebetouw, R., & Wood, K. 2007, *ApJS*, 169, 328
- Rowan-Robinson, M., Babbedge, T., Surace, J., et al. 2005, *AJ*, 129, 1183
- Strom, K. M., Strom, S. E., Kenyon, S. J., & Hartmann, L. 1988, *AJ*, 95, 534

TABLE 1  
CANDIDATE YOUNG STELLAR OBJECTS IN THE PIPE NEBULA

no.	RA, Dec (J2000) <sup>a</sup>	core	core mass [ $M_{\odot}$ ]	$A_V$ <sup>b</sup> [mag]	$A_V$ <sup>c</sup> [mag]	MIPS70 [Jy]	err. [Jy]	$\Delta_{\text{pos}}^{\text{d}}$ [ $''$ ]	MIPS24 [Jy]	err. [Jy]	$F_{\nu}(70\ \mu\text{m})/$ $F_{\nu}(24\ \mu\text{m})$	ID <sup>e</sup>
1	17:11:23.09 -27:24:32.80	9	19.4	20.2	24.9	42.100	8.400	0.5	4.715	0.940	8.9	[BHB2007] 11
2	17:11:17.45 -27:25:08.48	9	19.4	11.1	15.0	10.100	0.709	3.6	9.200	1.840	1.1	[BHB2007] 7
3	17:11:22.12 -27:26:02.30	9	19.4	8.8	9.9	9.190	0.644	0.7	1.710	0.074	5.4	[BHB2007] 10
4	17:11:03.95 -27:22:55.39	7	4.0	4.2	7.9	8.490	0.596	0.6	6.320	1.260	1.3	[BHB2007] 1 <sup>f</sup>
5	17:10:08.20 -27:15:20.20	–	<0.1	2.4	3.0	2.901	0.203	1.5	6.100	1.250	0.5	KK Oph
6	17:11:21.43 -27:27:42.91	9	19.4	12.4	15.7	2.070	0.145	1.4	1.540	0.064	1.3	[BHB2007] 9
7	17:11:27.00 -27:23:49.05	9	19.4	10.5	18.1	1.780	0.125	0.6	0.831	0.034	2.1	[BHB2007] 13
8	17:11:18.13 -27:25:49.30	9	19.4	7.5	13.0	1.440	0.101	–	0.412	0.017	3.5	[BHB2007] 8
9	17:11:30.32 -27:26:29.57	9	19.4	10.3	14.4	1.310	0.092	0.9	0.150	0.006	8.7	[BHB2007] 16
10	17:35:02.22 -25:23:49.54	–	0.3	2.2	8.5	0.919	0.065	0.6	2.160	0.086	0.4	R
11	17:14:51.05 -27:22:41.02	17	1.6	2.2	5.6	0.817	0.058	0.8	0.550	0.022	1.5	Src 1 <sup>g</sup>
12	17:11:27.28 -27:25:28.99	9	19.4	12.4	20.3	0.710	0.050	1.5	0.455	0.018	1.6	[BHB2007] 14
13	17:29:41.64 -26:29:09.34	49	0.8	2.1	6.6	0.688	0.049	3.4	0.906	0.036	0.8	R
14	17:25:18.87 -26:46:07.79	40	4.2	1.7	5.1	0.669	0.047	2.5	1.237	0.049	0.5	R
15	17:36:57.59 -24:18:06.02	–	0.3	1.4	4.9	0.469	0.034	0.5	1.346	0.054	0.3	R
16	17:14:56.44 -27:31:09.26	–	0.5	1.5	4.1	0.323	0.023	0.2	0.416	0.017	0.8	R
17	17:37:35.42 -23:30:52.19	–	1.5	3.7	7.9	0.270	0.020	1.3	0.213	0.009	1.3	Src 2 <sup>g</sup>
18	17:11:29.31 -27:25:36.30	9	19.4	12.4	15.6	0.246	0.018	–	0.104	0.004	2.4	[BHB2007] 15
19	17:20:18.85 -26:55:57.35	29	4.3	1.4	4.8	0.241	0.017	1.8	0.014	0.001	16.7	R
20	17:34:01.76 -25:24:10.73	92	1.0	1.7	9.3	0.213	0.015	1.4	0.013	0.001	16.2	R
21	17:11:14.45 -27:26:54.40	9	19.4	7.5	11.8	0.210	0.016	–	0.155	0.006	1.4	[BHB2007] 4
22	17:23:35.15 -23:42:24.05	100	2.4	2.8	4.1	0.184	0.013	0.8	0.011	0.001	16.8	R
23	17:11:11.78 -27:26:55.17	9	19.4	9.0	12.9	0.110	0.009	1.4	0.095	0.004	1.2	[BHB2007] 3
24	17:20:54.17 -26:46:42.77	34	9.3	2.3	5.7	0.110	0.009	0.7	0.014	0.001	7.6	R
25	17:29:28.24 -25:56:25.08	57	2.8	3.9	8.6	0.104	0.008	2.6	0.014	0.001	7.6	R
26	17:19:41.25 -26:55:31.67	29	4.3	8.1	10.6	–	–	–	0.163	0.007	–	–

NOTE.—Sources sorted according to their 70  $\mu\text{m}$  flux. Photometry for Barnard 59 sources is from Brooke et al. (2007).

<sup>a</sup>from MIPS 24  $\mu\text{m}$  data except for sources 8, 18 and 21, which were added from Brooke et al. (2007), see text

<sup>b</sup>optical extinction from an extinction map with extended structure removed (Alves et al. 2007)

<sup>c</sup>optical extinction from an extinction map including extended structure (Lombardi et al. 2006)

<sup>d</sup>distance between MIPS70 and MIPS24 positions in source detection, possibly misleading for bright sources

<sup>e</sup>R = rejected candidate YSO (see text)

<sup>f</sup>at MIPS wavelengths: blend with neighboring [BHB2007] 2; pair also known as LkH $\alpha$  346 AB.

<sup>g</sup>in Covey et al. 2009 (in prep.)

TABLE 2  
CANDIDATE YOUNG STELLAR OBJECTS IN THE PIPE NEBULA: 2MASS COUNTERPARTS

no.	2MASS name	2MASS- <i>J</i> [mag]	err. [mag]	2MASS- <i>H</i> [mag]	err. [mag]	2MASS- <i>K<sub>S</sub></i> [mag]	err. [mag]
1	J17112317-2724315	>18.78	–	>17.80	–	15.08	0.14
2	J17111726-2725081	13.62	0.04	10.82	0.04	8.77	0.03
3		–	–	–	–	–	–
4	J17110392-2722551	10.46	0.03	8.99	0.03	7.76	0.02
5	J17100811-2715190	9.07	0.03	7.23	0.04	5.80	0.03
6	J17112153-2727417	12.74	0.02	10.57	0.02	8.98	0.03
7	J17112701-2723485	11.88	0.04	10.14	0.04	9.08	0.03
8	J17111827-2725491	>18.4	–	15.12	0.08	11.95	0.03
9	J17113036-2726292	11.91	0.03	10.00	0.03	8.89	0.02
10	J17350225-2523503	15.55	0.07	14.34	0.08	13.11	0.06
11	J17145108-2722399	10.26	0.02	8.89	0.02	8.16	0.02
12	J17112729-2725283	13.17	0.03	10.65	0.03	9.11	0.02
13	J17294185-2629092	13.75	0.04	10.06	0.02	7.63	0.02
14	J17251886-2646099	>16.05	–	13.23	0.04	9.72	0.03
15	J17365757-2418066	>12.71	–	10.65	0.06	8.40	0.03
16	J17145648-2731080	10.42	0.02	9.56	0.03	9.04	0.02
17	J17373543-2330517	14.60	0.05	12.38	0.04	10.92	0.03
18	J17112942-2725367	13.28	0.02	11.74	0.02	10.70	0.02
19		–	–	–	–	–	–
20	J17340187-2524070	15.71	0.08	14.02	0.07	13.31	0.06
21	J17111445-2726543	11.62	0.02	10.42	0.02	9.63	0.02
22	J17233513-2342249	16.10	0.11	15.06	0.10	14.39	0.10
23	J17111182-2726547	14.09	0.03	12.62	0.03	11.76	0.03
24	J17205433-2646434	12.30	0.02	11.02	0.02	10.46	0.03
25	J17292824-2556252	9.01	0.03	7.93	0.03	7.47	0.03
26	J17194124-2655317	>18.35	–	>15.86	–	14.57	0.08

NOTE.—Sources 3 and 19 do not have 2MASS counterparts.

TABLE 3  
COMPARISON OF DETECTIONS IN THE HIGH-EXTINCTION REGIONS AND THE CONTROL REGIONS

	control region N	scaled to high-ext. area N	high-ext. region N
"class I"	48	2.9	9
"class II"	64	4.0	16
"class III"	87	5.2	9

NOTE.—The designations in the first column correspond to the flux space regions shown in Figures 1 and 2.

TABLE 4  
FIT RESULTS FOR CANDIDATE YOUNG STELLAR OBJECTS IN THE PIPE NEBULA

Source	$A_V(\text{tot})$ mag min	mag max	$L_{\text{bol}}$ $L_{\odot}$ min	$L_{\odot}$ max	$\alpha_{K-24}$	class <sup>a</sup>
1	116.7	179.9	1.4	2.6	2.71	I
2	20.7	117.7	16.5	30.1	0.58	I
3	78.2	996.9	0.7	20.1	–	I
4	8.1	106.3	7.0	29.6	0.03	f
5	8.7	62.9	55.9	175.4	-0.73	II
6	14.1	24.7	2.4	11.5	-0.09	f
7	8.9	12.8	0.7	2.7	-0.30	f
8	40.1	48.1	1.4	12.3	0.50	I
9	9.3	13.8	0.5	4.5	-1.09	II
11	4.3	34.0	0.8	6.6	-0.83	II
12	15.3	22.4	1.0	7.6	-0.54	II
16	1.9	14.8	0.6	2.5	-0.61	II
17	15.0	16.4	0.3	0.6	-0.17	f
18	6.6	36.7	0.1	0.8	-0.55	II
21	4.5	21.9	0.2	1.1	-0.79	II
23	9.5	26.4	0.1	0.2	-0.18	f
24	1.1	3.2	0.1	0.2	-1.47	II
26	30.0	31.7	0.3	0.3	1.12	I

NOTE.—For source 9, the goodness-of-fit criterion has been relaxed to allow for more than one fit (see text).

<sup>a</sup>evolutionary class, determined from the full SEDs;  $\alpha_{K-24}$  is used to differentiate flat-spectrum from class I and II sources (Greene et al. 1994):  $\alpha \geq 0.3 \rightarrow$  class I;  $-0.3 \leq \alpha < 0.3 \rightarrow$  class f (flat spectrum); and  $\alpha < -0.3 \rightarrow$  class II

Young, C. H., Jørgensen, J. K., Shirley, Y. L.,  
et al. 2004, ApJS, 154, 396

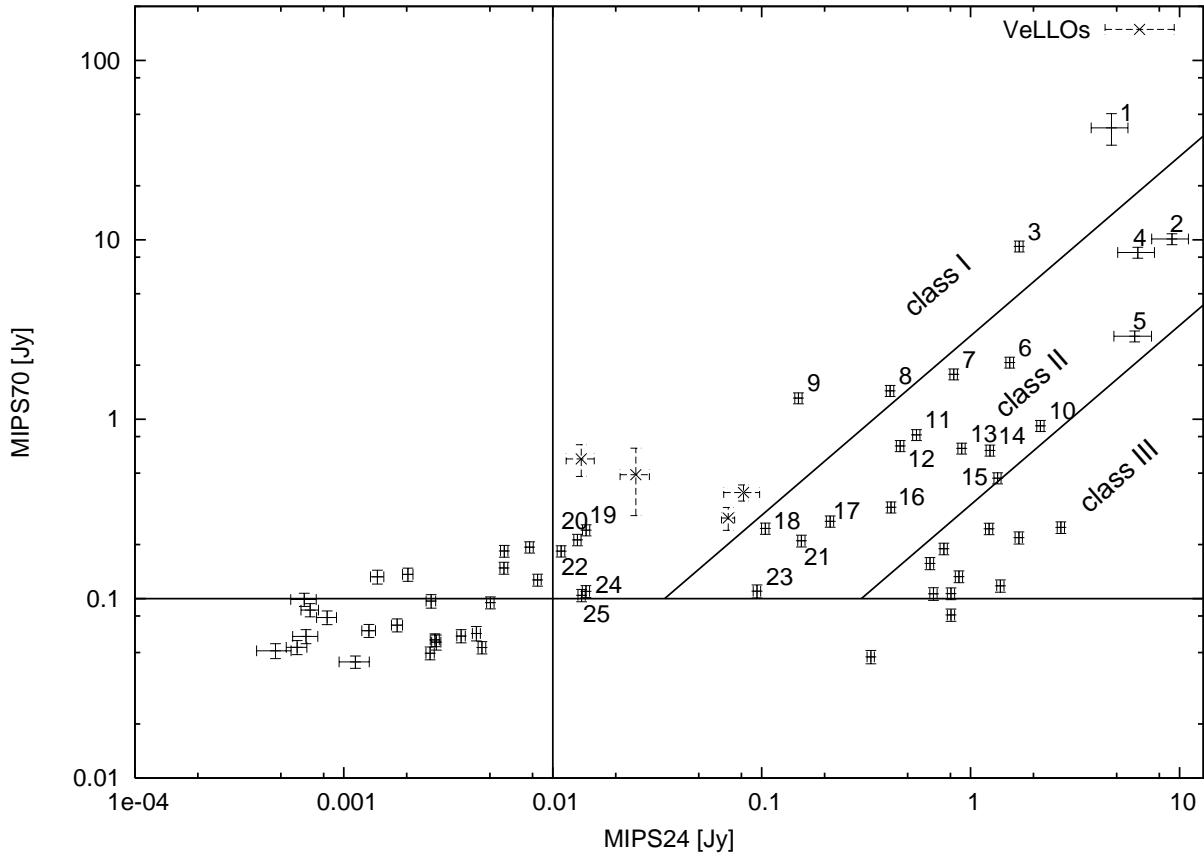


Fig. 1.— Plot of the MIPS fluxes of sources in the high-extinction regions. Regions where we expect to find candidate Young Stellar Objects in various evolutionary stages are marked. The boundaries of these regions were adapted from the original definition of YSO classes at shorter wavelengths, as discussed in Section 3.1. Dashed error bars denote the four VeLLOs that have been studied in detail (see text).

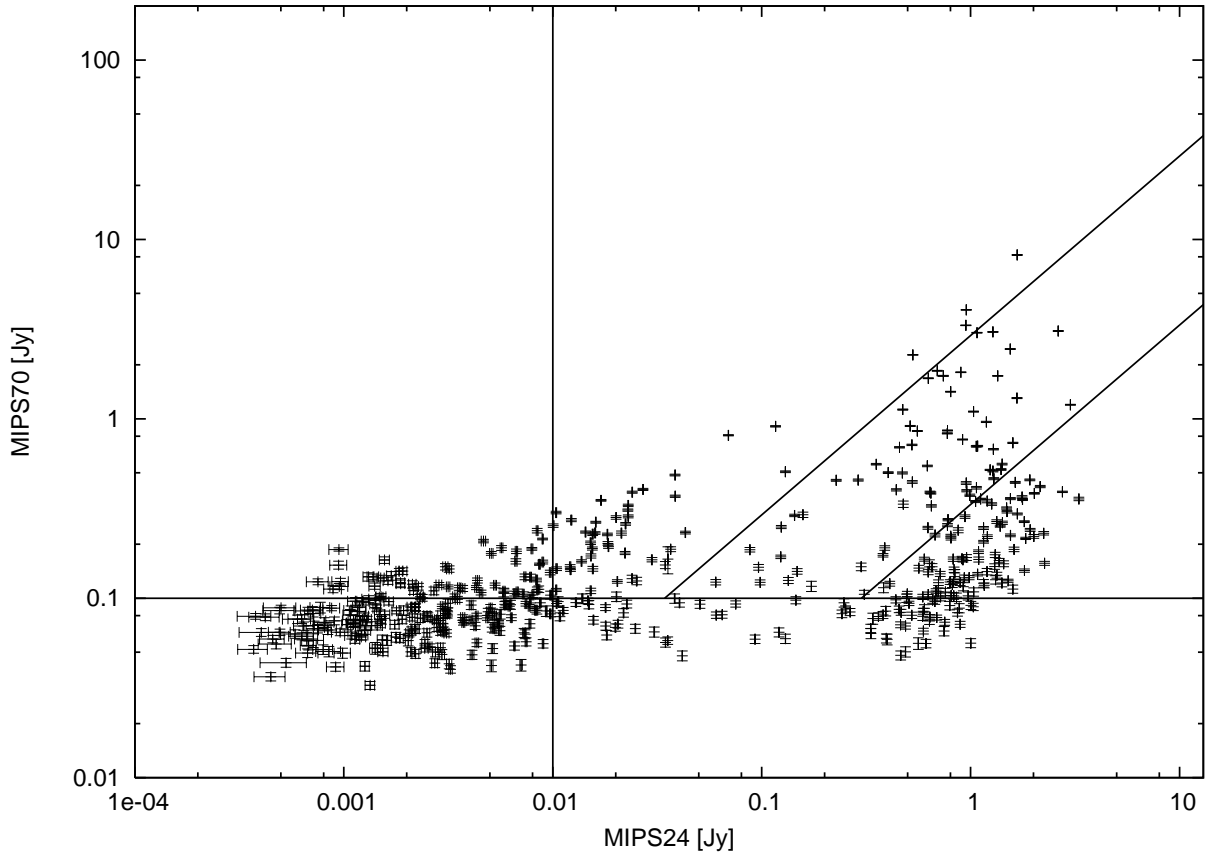


Fig. 2.— Plot of the MIPS fluxes of sources in the control region of the maps, outside of the high-extinction regions ( $A_V < 1.2$ ). The areas used for the identification of candidate Young Stellar Objects are marked, as in Fig. 1, even though we only use this plot to determine the background contamination.

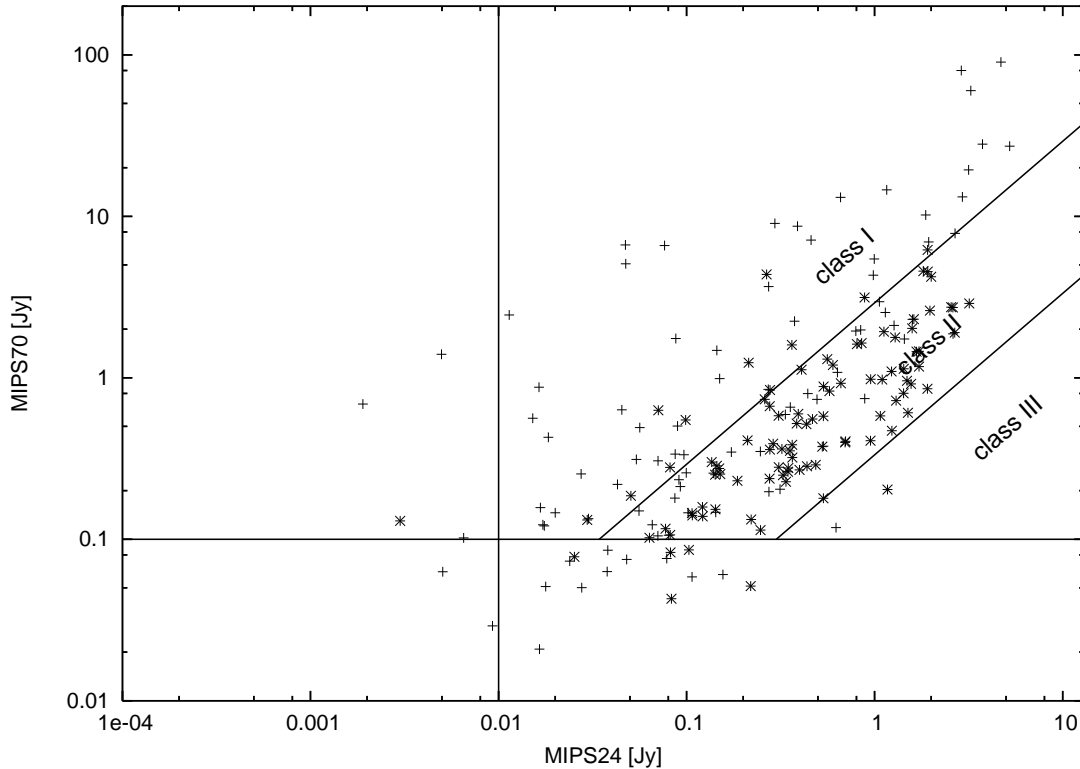


Fig. 3.— Plot of the MIPS sources in other star forming regions: ‘+’ symbols mark MIPS sources among the candidate YSOs from the ensemble list of cores produced by the Cores to disks Spitzer Legacy Project. The lines denote the same selection regions that we also used for the Pipe candidate YSOs. Note that the plot contains objects from star-forming regions at different distances, without a correction for this effect. Asterisks mark the MIPS fluxes of counterparts to YSOs in Taurus-Auriga, as listed by Kenyon et al. (2008), see text. For comparison, the flux regions for our YSO selection are shown. Both the c2d sources as well as the Taurus sources mostly fall into the area that we use for candidate YSO identification.



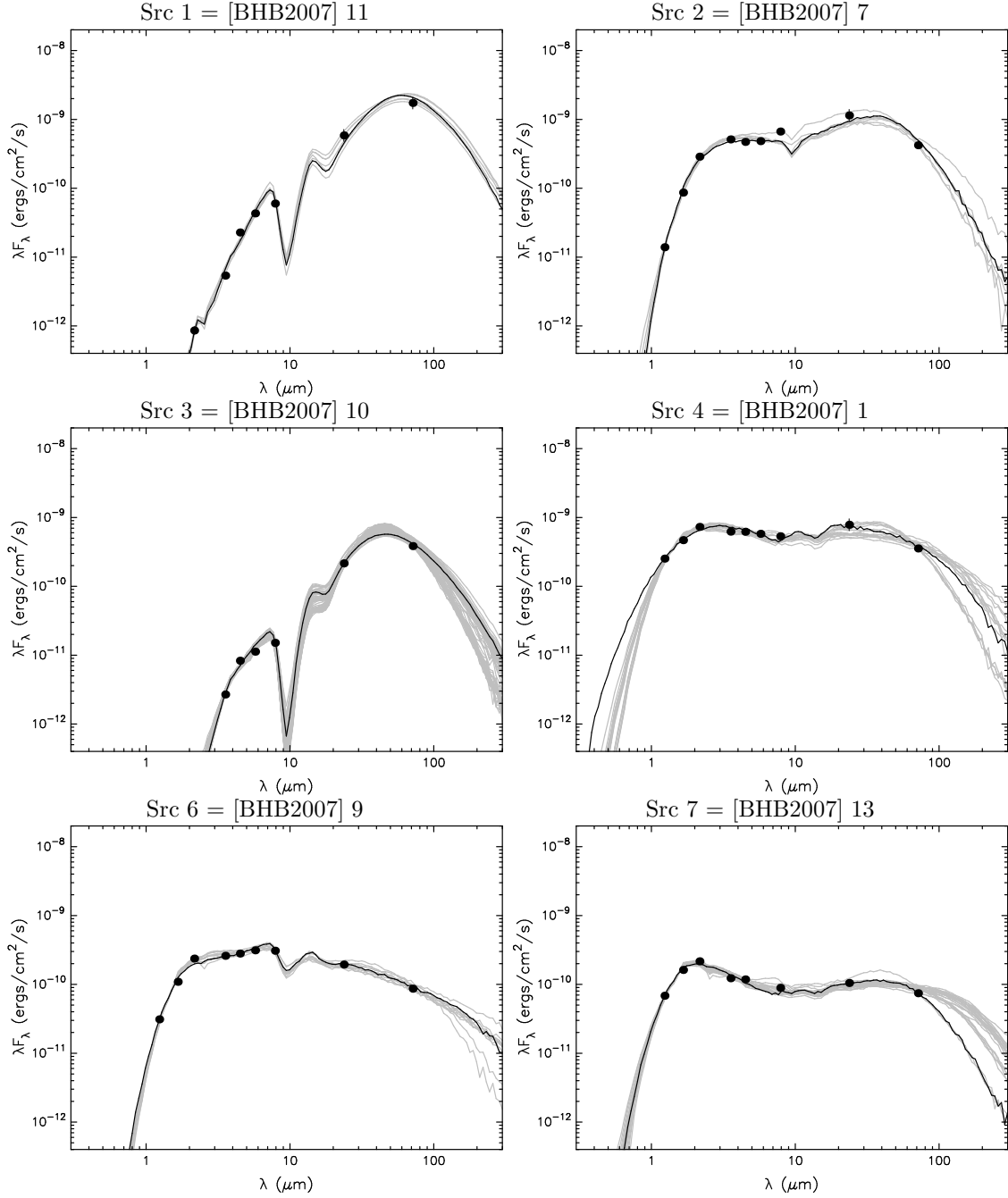


Fig. 4.— SEDs of candidate YSOs in B 59. The black line shows the best fit with gray lines delineating alternative fits within the goodness-of-fit criterion used (see text). Note that for Source 9, this criterion had to be relaxed.

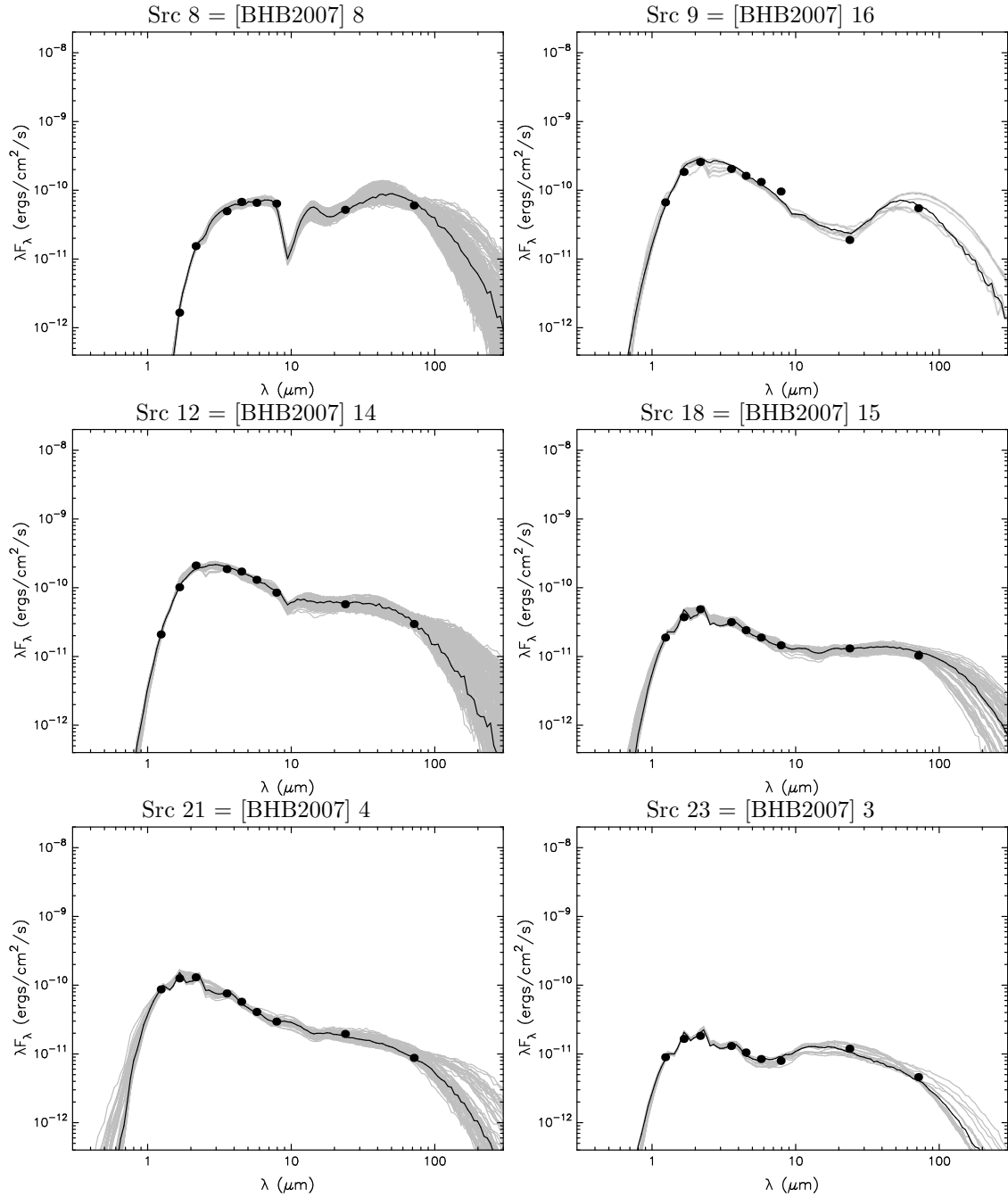


Fig. 4 – cntd.

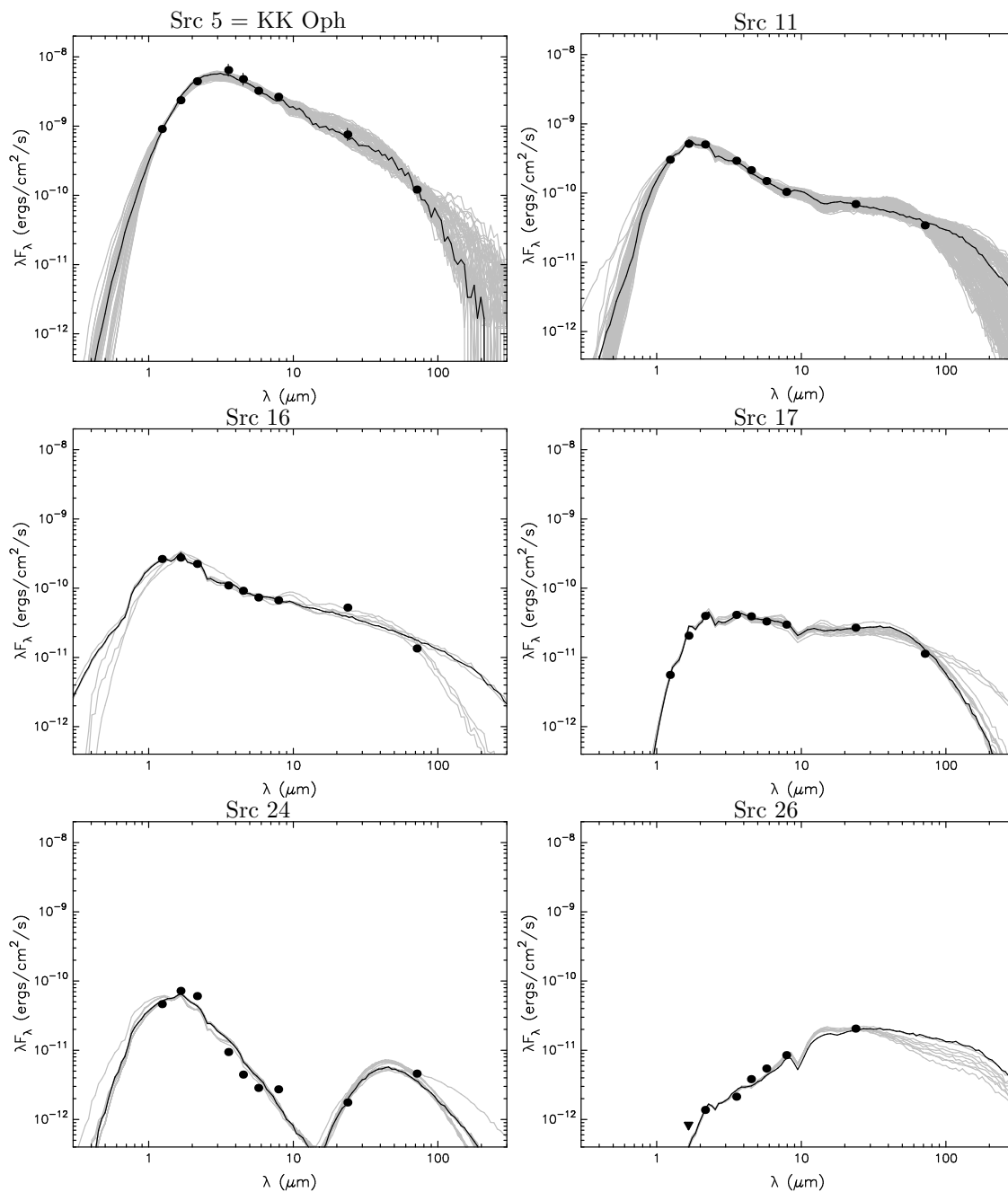


Fig. 5.— SEDs for candidate YSOs outside of B 59

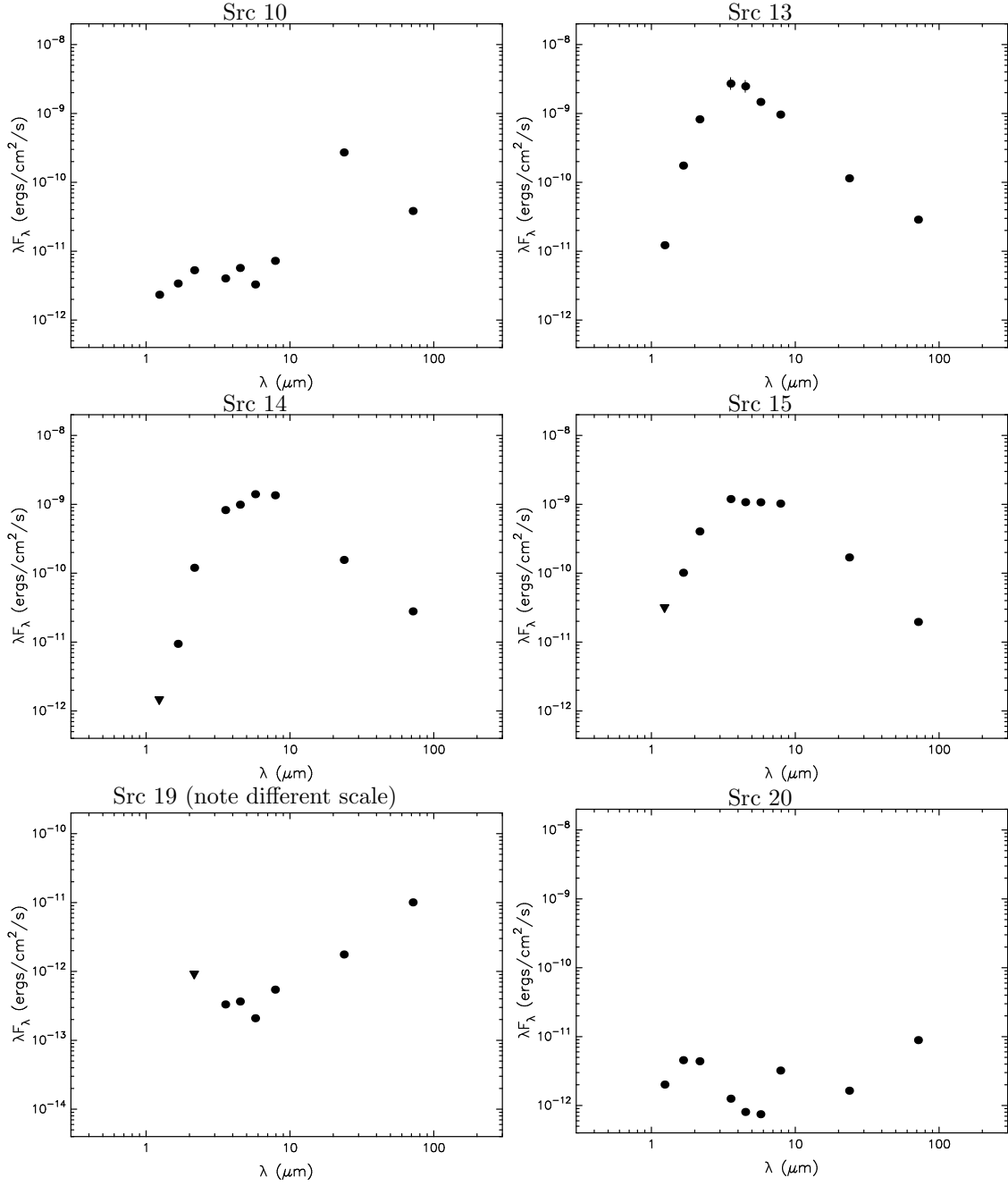


Fig. 6.— SEDs of rejected candidate YSOs and four sample control sources that fulfill the YSO selection criteria (designated only with their coordinates).

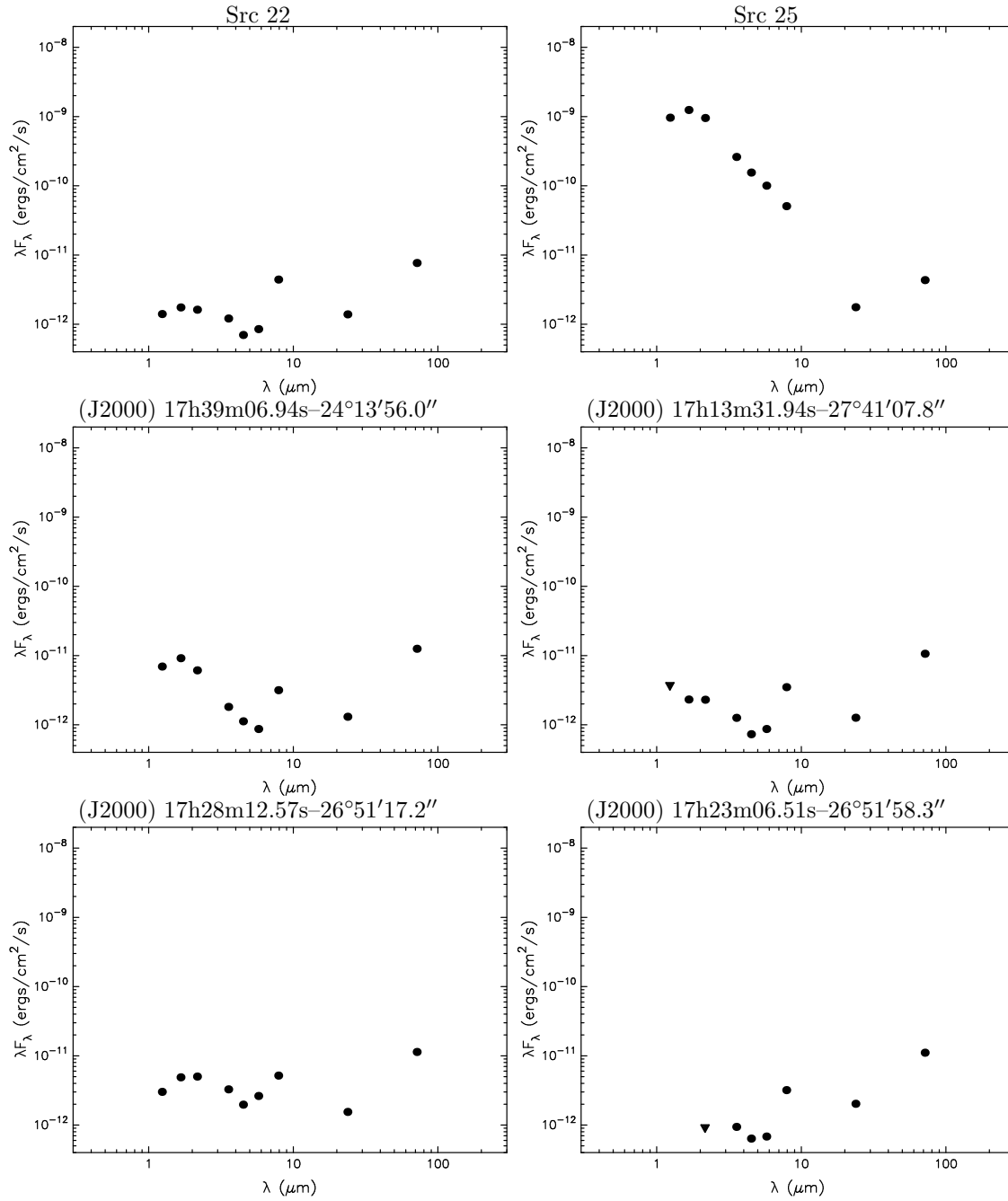


Fig. 6 – cntd.

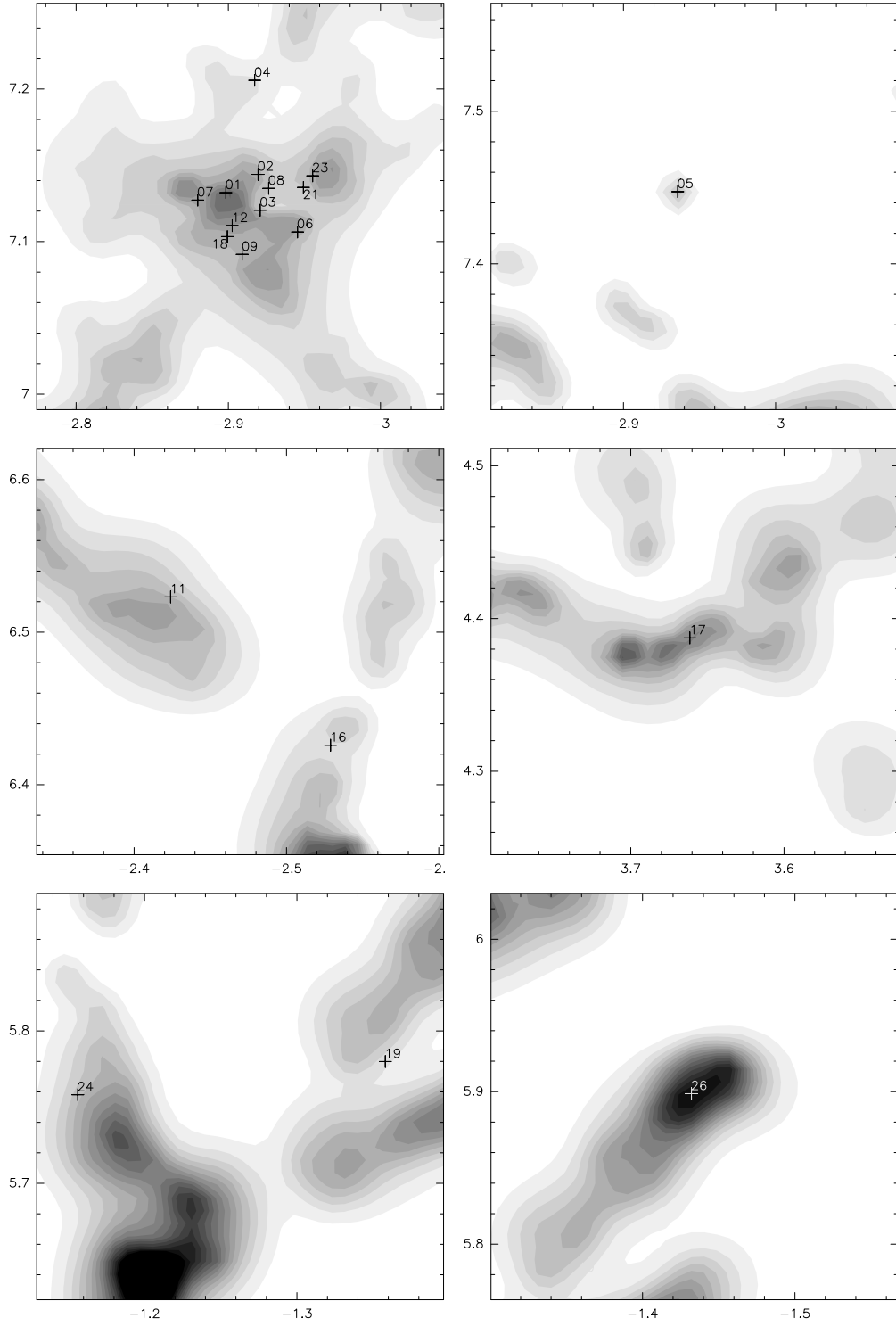


Fig. 7.— Location of the identified candidate YSOs relative to extinction peaks. Extinction is shown in shades of grey, starting at  $A_V < 1.2$  and advancing in steps of 0.5. Due to its high extinction, the B59 region is instead shown in an  $A_V$  range from 2 to 20 in steps of 2. The coordinates are Galactic coordinates.

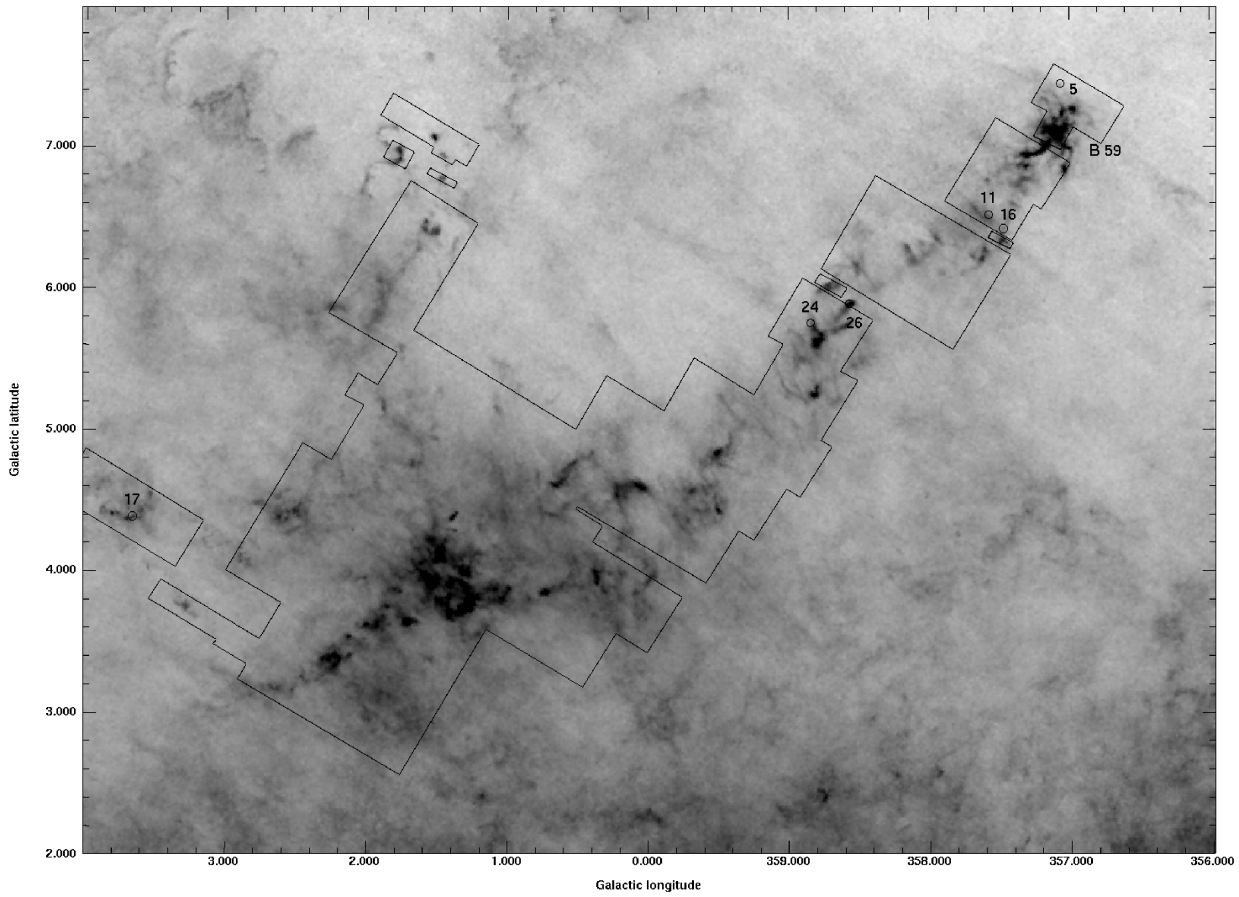


Fig. 8.— Location of the identified candidate YSOs on the full extinction map from Lombardi et al. (2006). Due to the high source density in B 59, only the location of the cluster is indicated. The approximate outline of the combined *Spitzer*-MIPS coverage ( $24\ \mu\text{m}$  and  $70\ \mu\text{m}$ ) is marked. For details, see Fig. 7.